International Journal of Solids and Structures 47 (2010) 2525–2532

Contents lists available at ScienceDirect

International Journal of Solids and Structures

journal homepage: www.elsevier.com/locate/ijsolstr

Mechanics of shaft-loaded blister test for thin film suspended on compliant substrate

MingHao Zhao [a,b,*], WeiLing Zheng [b], CuiYing Fan [a]

[a] The School of Mechanical Engineering, Zhengzhou University, No. 100 Science Road, Zhengzhou, Henan 450001, China
[b] Department of Engineering Mechanics, Zhengzhou University, No. 100 Science Road, Zhengzhou, Henan 450001, China

ARTICLE INFO

Article history:
Received 6 February 2010
Received in revised form 5 May 2010
Available online 19 May 2010

Keywords:
Shaft-loaded blister test
Thin film
Compliant substrate
Residual stress
Deflection
Analytical solution
Numerical solution

ABSTRACT

Based on the von Kármán plate theory, the mechanics of a shaft-loaded blister test for thin film/substrate systems is studied by considering elastic substrate deformations and residual stresses in these films. In testing, films are attached to a substrate provided with a circular hole, through which loading is applied to the film by a flat-ended shaft of circular cross-section. The effect of substrate deformation on the deflection of the loaded film is taken into account by using a line spring model. For small deflections, an analytical solution is derived, while for large deflections a numerical solution is obtained using the shooting method. The resulting load-shaft displacement relation, which is essential in blister tests, compares favorably with finite element analysis.

1. Introduction

The basis of microelectromechanical systems (MEMS) is thin film manufacturing. The mechanical properties of thin films determine, to a large extent, the reliability of MEMS. Material parameters, such as Young's modulus, residual stress and interfacial fracture toughness are essential and necessary input information to enable detailed design and analysis of MEMS devices to be developed. Due to their small dimensions, however, their mechanical properties are difficult to measure by conventional techniques. Various experimental methods were developed to measure these mechanical properties (Volinsky et al., 2002), such as the bulge/blister test (Dannenberg, 1961; Williams, 1969), the indentation test (Marshall and Evens, 1984; Pharr and Oliver, 1992; Li and Chou, 1997; Antunes et al., 2007), the scratch test (Randall et al., 2001), the microcantilever-beam test (Weihs et al., 1988), the microbridge test (Zhang et al., 2000a), and many others.

Among the available methods, the bulge/blister test has been widely used in measuring Young's modulus and interfacial fracture toughness between film and its associated substrate (Dannenberg, 1961; Williams, 1969). In earlier tests, deflections and debondings were caused by applying hydrostatic pressure. One disadvantage, however, is that the strain energy release rate increases as blister radius increases and debondings become unstable (Lai and Dillard, 1994). Moreover, pressurized blister tests require sophisticated experimental equipment to monitor the simultaneous change in blister dimension and dissolved gases may invalidate such tests (Wan, 1999). Shaft-loaded blister tests offer an alternative to pressured blister tests because a universal test machine can drive the shaft that induces displacements. Two models of shaft-loading blister testing exist; one based on Föppl–Hencky equations, the other on von Kármán plate theory. Föppl (1907) and Hencky (1915) developed the central point-loaded Föppl–Hencky equations under the assumptions that the strains are sufficiently small so that linear stress–strain relations are approximately valid and that rotations are sufficiently restricted. Recently, Jin and Wang (2008) derived exact solutions for the nonlinear regime of large deflections of a thin circular membrane loaded by a central point force with two types of boundary conditions (i.e., loosely and rigidly clamped edges) and with or without residual stress. Considering both bending and nonlinear stretching effects using the von Kármán plate theory, which we employ below, Wan (1999) reported strain energy release rates for a pointed loaded plate. Wan and Liao (1999) used a rigid spherically-capped shaft for a clamped circular plate in their blister tests. In considering the effect of residual stress within the film, Wan et al. (2003) and Xu et al. (2003) obtained approximate analytical solutions for a clamped circular plate. Jin (2008) presented a theoretical study of shaft-load blister testing to determine the energy release rate

* Corresponding author at: The School of Mechanical Engineering, Zhengzhou University, No. 100 Science Road, Zhengzhou, Henan Province 450001, China. Tel.: +86 371 67739058; fax: +86 371 67781786.
E-mail addresses: memhzhao@zzu.edu.cn, memhzhao@sina.com (M. Zhao).

0020-7683/$ - see front matter © 2010 Elsevier Ltd. All rights reserved.
doi:10.1016/j.ijsolstr.2010.05.011

and bending to stretching behavior of thin polymer films and coatings on rigid substrates. Kozlova et al. (2008) used the shaft-load blister method to study copper/alumina joints brazed with a CuAg-Ti alloy. Very recently, Xiao et al. (2009) developed a novel blister test theory model based on the bending theory of beams to assess the interface strength between nickel film and low carbon steel substrate under loads applied with a flat-end shaft.

In existing models, however, the circular film was clamped along the boundary. The substrate was treated as rigid or non-deformable but, as is well known, an elastic substrate will deform when a film is deflected. The compliance of a substrate has a significant influence on film deformation and debonding behavior of the film from its substrate, which has been studied intensively and extensively in the buckling and cracking of thin films (Cotterell and Chen, 2000), in microbridge tests (Zhang et al., 2000a), in microcantilever bending tests (Zhang et al., 2000b), and in analyses of straight-sided delamination buckling (Yu and Hutchinson, 2002; Zhao et al., 2007a).

Motivated by the above background, we report here on the mechanics of shaft-loaded blister tests focusing particularly on substrate deformation and residual stress. Following this introduction, the governing equation will be given in Section 2. In Section 3, a coupled line spring is described that models the compliance of the substrate and the boundary conditions along the edge of the deflected part of the film. In Section 4, the normalized governing equations and the boundary conditions are presented. An analytical solution for small deflections is derived in Section 5, and a numerical solution for large deflections is presented in Section 6. Section 7 concludes the paper with some final remarks.

2. Governing equations

A thin film of thickness h is attached to its substrate with a circular hole of radius a. The shaft-loaded blister test set-up is schematically shown in Fig. 1a. A circular flat-ended shaft of radius $b < a$ is used to apply a downward force denoted by P_0. Because of axial symmetry, the cylindrical coordinate system orz is used as illustrated in Fig. 1a. The deformation of the loaded film is shown schematically in Fig. 1b. If the thin film has rigidity against bending and the loading is sufficiently large, the contact area is annular due to the elastic deformation of the thin film (Wan and Liao, 1999). Based on the von Kármán plate theory, the basic governing equations of the loaded film are given by

$$D\frac{1}{r}\frac{d}{dr}\left\{r\frac{d}{dr}\left[\frac{1}{r}\frac{d}{dr}\left(r\frac{dw}{dr}\right)\right]\right\}-\frac{1}{r}\frac{d}{dr}\left(rN_r\frac{dw}{dr}\right)=\frac{P_0\delta(r-b)}{2\pi b}, \tag{1}$$

$$r^2\frac{d^2N_r}{dr^2}+3r\frac{dN_r}{dr}+\frac{E_fh}{2}\left(\frac{dw}{dr}\right)^2=0, \tag{2}$$

where $w(r)$ is the vertical deflection, D is the flexural rigidity given by $D=\frac{E_fh^3}{12\left(1-\nu_f^2\right)}$, E_f and ν_f are, respectively, Young's modulus and the Poisson ratio of the film, with subscript "f" referring to the film. δ is the Dirac delta function, and N_r is the radial force per unit width in the film expressed as

$$N_r=N_0+\Delta N_r,\quad N_0=\sigma_0h, \tag{3}$$

where σ_0 is the residual stress uniformly distributed in the film, and ΔN_r is the change in radial force due to the deflection of the film by the applied force P_0.

Integrating Eq. (1) yields

$$D\frac{d}{dr}\left[\frac{1}{r}\frac{d}{dr}\left(r\frac{dw}{dr}\right)\right]-N_r\frac{dw}{dr}=\frac{P_0H(r-b)}{2\pi r}+\frac{C}{r}, \tag{4}$$

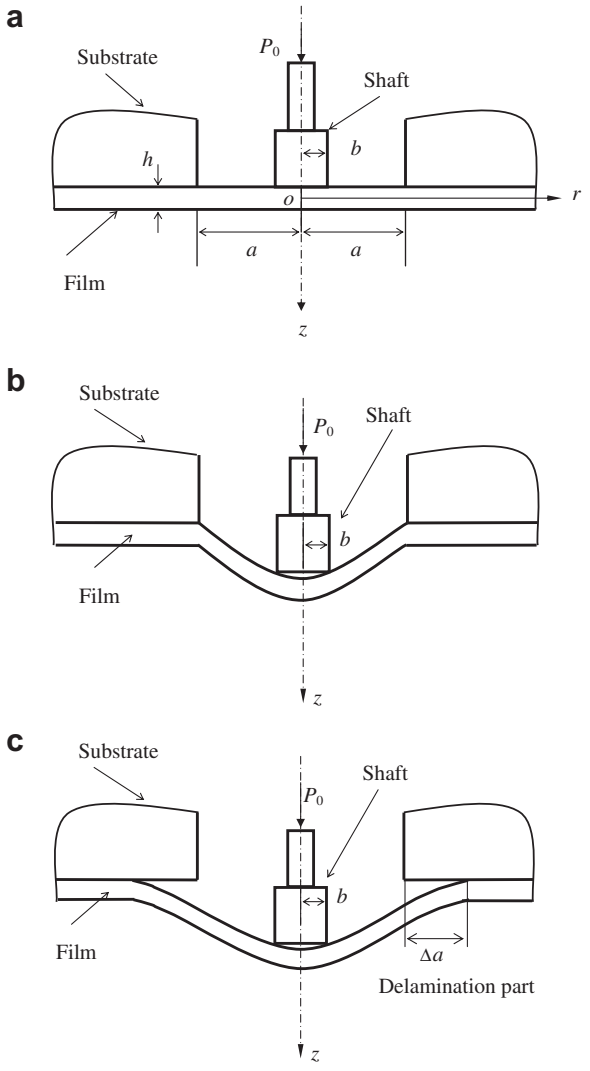

Fig. 1. (a) Shaft-loaded blister test of a circular thin film/substrate system. (b) Deformation of the loaded thin film. (c) Delamination of the loaded thin film.

where C is a constant to be determined, and $H(r-b)$ is the Heaviside function,

$$H(r-b)=\begin{cases}0, & r<b,\\ 1, & r\geqslant b.\end{cases} \tag{5}$$

In the von Kármán plate theory, the shear force is expressed as

$$Q=-D\frac{d}{dr}\left[\frac{1}{r}\frac{d}{dr}\left(r\frac{dw}{dr}\right)\right]. \tag{6}$$

Substituting Eq. (6) into Eq. (4) leads to

$$-Q-N_r\frac{dw}{dr}=\frac{P_0H(r-b)}{2\pi r}+\frac{C}{r}. \tag{7}$$

Considering the conditions in the center of the film,

$$\frac{dw}{dr}=0,\quad Q=0, \tag{8}$$

one obtains

$$C=0. \tag{9}$$

Finally, Eq. (4) is rewritten as

$$D\left(r^2\frac{d^2\phi}{dr^2}+r\frac{d\phi}{dr}-\phi\right)-r^2(N_0+\Delta N_r)\phi=\frac{P_0 rH(r-b)}{2\pi}, \tag{10}$$

where $\phi=\frac{dw}{dr}$ is the rotation.

When the applied load is sufficiently large, the film separates from the substrate as depicted in Fig. 1c and as observed in the test method by Xiao et al. (2009). The radius of the newly formed blister is $a_N = a + \Delta a$.

3. The coupled line spring model and the boundary conditions

3.1. The coupled line spring model of the substrate deformation

The substrate deforms when the film is deflected by the shaft. The coupling between the substrate deformation and the deflected circular film can be modeled by coupled line springs (Zhang et al., 2000a; Zhao et al., 2007a). If the thin plate is detached from the system along the edge of the join between substrate and film, as shown in Fig. 2, the coupling of the remaining film/substrate system with the detached portion of the thin film can be modeled as coupled line springs and the constitutive equations are given by Zhang et al. (2000a,b)

$$\begin{bmatrix}u_s\\ w_s\\ \phi_s\end{bmatrix}=\begin{bmatrix}S_{NN} & S_{NQ} & S_{NM}\\ S_{QN} & S_{QQ} & S_{QM}\\ S_{MN} & S_{MQ} & S_{MM}\end{bmatrix}\begin{bmatrix}N_s\\ Q_s\\ M_s\end{bmatrix}, \tag{11}$$

where the subscript "s" refers to the substrate. Q_s, M_s and N_s denote, respectively, the shear force, bending moment and the radial force, while u_s, w_s and ϕ_s represent, respectively, the radial displacement, the transversal displacement and the rotation angle. The S_{ij} with differing subscripts N, Q and M are the generalized compliances that depend on the properties and geometric parameters of both film and substrate, including Young's moduli and the Poisson ratios of the film and substrate, E_f, E_s, v_f and v_s, and the ratio a/h. According to dimensional analysis, the compliance coefficients are normalized by Zhao et al. (2007b)

$$S_{NN}=\frac{C_{NN}}{\overline{E}_f},\quad S_{NQ}=\frac{C_{NQ}}{\overline{E}_f}=\frac{C_{QN}}{\overline{E}_f}=S_{QN},\quad S_{NM}=\frac{C_{NM}}{\overline{E}_f h}=\frac{C_{MN}}{\overline{E}_f h}=S_{MN},$$

$$S_{QQ}=\frac{C_{QQ}}{\overline{E}_f},\quad S_{MQ}=\frac{C_{MQ}}{\overline{E}_f h}=\frac{C_{QM}}{\overline{E}_f h}=S_{QM},\quad S_{MM}=\frac{C_{MM}}{\overline{E}_f h^2}. \tag{12}$$

In Appendix, we give expressions for the normalized compliance coefficients C_{ij} with differing subscripts N, Q and M as functions of a/h and the Dundurs parameters defined as

$$\alpha=\frac{\overline{E}_f-\overline{E}_s}{\overline{E}_f+\overline{E}_s},$$
$$\beta=\frac{1}{2}\frac{\overline{E}_f(1-v_f)(1-2v_s)-\overline{E}_s(1-2v_f)(1-v_s)}{\overline{E}_f(1-v_f)(1-2v_s)+\overline{E}_s(1-2v_f)(1-v_s)}, \tag{13}$$

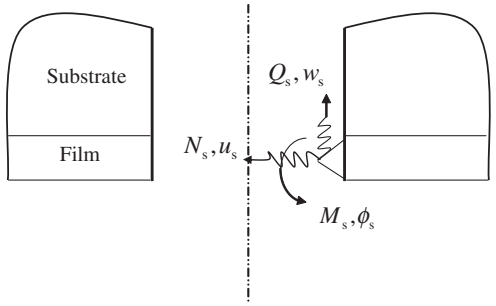

Fig. 2. Coupled line springs modeling substrate deformation.

where

$$\overline{E}_f=\frac{E_f}{1-v_f^2},\quad \overline{E}_s=\frac{E_s}{1-v_s^2}. \tag{14}$$

The parameter α defines the stiffness of a film relative to its substrate. Eq. (13) indicates that $\alpha = -1$ is to be interpreted as a film on a rigid substrate, while a positive value of α signifies that the film is harder than the associated substrate. The influence of parameter β is negligible compared with α (Yu and Hutchinson, 2002; Zhao et al., 2007a), and therefore we set $\beta = 0$ throughout this paper.

The positive definiteness of energy requires that

$$C_{MQ}=C_{QM},\quad C_{MN}=C_{NM},\quad C_{NQ}=C_{QN}. \tag{15}$$

3.2. The boundary conditions

The bending moment and shear force in the film are expressed in terms of the deflection or rotation

$$M=-D\left[\frac{d\phi}{dr}+\frac{v_f}{r}\phi\right], \tag{16}$$

$$Q=-D\frac{d}{dr}\left[\frac{d\phi}{dr}+\frac{\phi}{r}\right]. \tag{17}$$

The constitutive equation gives the radial displacement

$$u=\frac{r}{E_f h}\left[r\frac{d\Delta N_r}{dr}+(1-v_f)\Delta N_r\right]. \tag{18}$$

Along the edge of the circular film, we have conditions

$$u=-u_s,\quad \phi=-\phi_s,\quad w=-w_s, \tag{19a}$$

$$\Delta N_r=N_s,\quad M=-M_s,\quad Q=Q_s,\quad \text{at } r=a, \tag{19b}$$

$$Q=-\frac{P_0}{2\pi a}. \tag{19c}$$

Substituting Eqs. (16)–(19) into Eq. (11) yields

$$\begin{aligned}-u&=S_{NN}\Delta N_r-S_{NQ}\frac{P_0}{2\pi a}+S_{NM}D\left[\frac{d\phi}{dr}+\frac{v_f}{r}\phi\right],\\ -w&=S_{QN}\Delta N_r-S_{QQ}\frac{P_0}{2\pi a}+S_{QM}D\left[\frac{d\phi}{dr}+\frac{v_f}{r}\phi\right],\quad \text{at } r=a,\\ -\phi&=S_{MN}\Delta N_r-S_{MQ}\frac{P_0}{2\pi a}+S_{MM}D\left[\frac{d\phi}{dr}+\frac{v_f}{r}\phi\right].\end{aligned} \tag{20}$$

At the center of the film, one has the boundary conditions

$$\phi=0,\quad \frac{d\Delta N_r}{dr}=0,\quad \text{at } r=0, \tag{21}$$

with a finite w imposed as a supplementary condition.

4. The normalized governing equations and the boundary conditions

Introducing the dimensionless parameters,

$$x=\frac{r}{a},\quad x_0=\frac{b}{a},\quad \varphi=\frac{a}{h}\phi,\quad P=\frac{a^2P_0}{2\pi Dh},\quad n=\sqrt{\frac{N_0a^2}{D}},$$
$$N_0>0, \tag{22a}$$

$$W(x)=\frac{w(r)}{h},\quad \Delta N=\frac{\Delta N_r a^2}{D},\quad N=\frac{N_r a^2}{D},\quad t=\frac{h}{a},$$
$$x_1=nx_0, \tag{22b}$$

the governing Eqs. (2) and (10) are normalized as

$$x^2\frac{d^2\varphi}{dx^2}+x\frac{d\varphi}{dx}-\varphi-x^2(\Delta N+N_0)\varphi=xPH(x-x_0), \tag{23a}$$

$$x^2\frac{d^2\Delta N}{dx^2}+3x\frac{d\Delta N}{dx}+6\left(1-v_f^2\right)\varphi^2=0, \tag{23b}$$

while the normalized boundary conditions in Eqs. (20) and (21) are given by

$$\begin{aligned}&\Delta N'+C_1\Delta N-C_2P+C_3[\varphi'+v_f\varphi]=0,\\ &W+C_4\Delta N-C_5P+C_6[\varphi'+v_f\varphi]=0,\quad \text{at } x=1\\ &\varphi+C_7\Delta N-C_8P+C_9[\varphi'+v_f\varphi]=0,\end{aligned} \tag{24a}$$

$$\varphi=0,\quad \frac{d\Delta N}{dr}=0,\quad \text{at } x=0, \tag{24b}$$

where

$$\begin{aligned}&C_1=1-v_f+C_{NN}\left(1-v_f^2\right)t,\quad C_2=C_{NQ}\left(1-v_f^2\right)t^2,\\ &C_3=C_{NM}\left(1-v_f^2\right)t,\\ &C_4=\frac{C_{NQ}}{12}t^2,\quad C_5=\frac{C_{QQ}}{12}t^3,\quad C_6=\frac{C_{QM}}{12}t^2,\\ &C_7=\frac{C_{NM}}{12}t,\quad C_8=\frac{C_{QM}}{12}t^2,\quad C_9=\frac{C_{MM}}{12}t.\end{aligned} \tag{25}$$

It can be seen that Eqs. (23a) and (23b) are nonlinear with respect to the radial force and rotation (or equivalently, deflection).

5. The analytical solution for the case of small deflection

5.1. The governing equations and the boundary conditions

For small deflections, the radial force is unchanged, i.e.,

$$\Delta N_r=N_s=0 \tag{26}$$

and the governing equation simplifies to

$$x^2\frac{d^2\varphi}{dx^2}+x\frac{d\varphi}{dx}-(1+n^2x^2)\varphi=0,\quad 0\leqslant x\leqslant x_0, \tag{27a}$$

$$x^2\frac{d^2\varphi}{dx^2}+x\frac{d\varphi}{dx}-(1+n^2x^2)\varphi=xP,\quad x_0\leqslant x\leqslant 1. \tag{27b}$$

The boundary conditions are given by

$$\begin{aligned}&W-C_5P+C_6[\varphi'+v_f\varphi]=0,\\ &\varphi-C_8P+C_9[\varphi'+v_f\varphi]=0,\end{aligned}\quad \text{at } x=1, \tag{28a}$$

$$\varphi=0,\quad \text{at } x=0. \tag{28b}$$

5.2. Solutions

The general solution to Eq. (27) can be expressed as

$$\varphi=c_1I_1(nx)+c_2K_1(nx),\quad 0\leqslant x\leqslant x_0, \tag{29a}$$

$$\varphi=c_3I_1(nx)+c_4K_1(nx)-\frac{P}{n^2x},\quad x_0\leqslant x\leqslant 1, \tag{29b}$$

where $I_n(\cdot)$ and $K_n(\cdot)$ are, respectively, the modified Bessel functions of the first and second kind of order n. The coefficients c_1, c_2, c_3 and c_4 are constants to be determined by the boundary conditions.

Substituting the general solution (29) into the boundary conditions (28), one can obtain

$$c_2=0, \tag{30}$$

$$c_4=\frac{P[x_1I_0(x_1)+2I_1(x_1)+x_1I_2(x_1)]}{nx_1k_1}, \tag{31}$$

$$c_3=k_2c_4+\frac{a_4P}{n^2(a_1I_0(n)+a_2I_1(n)+a_1I_2(n)+a_3I_3(n))}, \tag{32}$$

$$c_1=c_3+\frac{c_4K_1(x_1)nx_1-P}{nx_1I_1(x_1)}, \tag{33}$$

where

$$\begin{aligned}k_1=&K_1(x_1)(x_1I_0(x_1)+2v_fI_1(x_1)+x_1I_2(x_1))+I_0(x_1)(x_1K_0(x_1)\\&-2v_fK_1(x_1)+x_1K_2(x_1)),\end{aligned}$$

$$k_2=\frac{a_1K_0(n)-a_2K_1(n)+a_1K_2(n)-a_3K_3(n)}{a_1I_0(n)+a_2I_1(n)+a_1I_2(n)+a_3I_3(n)}. \tag{34}$$

Integrating Eq. (29) gives the deflection

$$W=c_1\frac{-1+I_0(nx)}{n}+c_5,\quad (0\leqslant x\leqslant x_0), \tag{35a}$$

$$W=c_3\frac{-1+I_0(nx)}{n}-c_4\frac{K_0(nx)}{n}-\frac{P\log x}{n^2}+c_6,\quad (x_0\leqslant x\leqslant 1). \tag{35b}$$

Substituting Eq. (35) into the first equation in Eq. (28) determines the constants

$$\begin{aligned}c_6=&c_3\left[\left(-\frac{1}{n}+a_7\right)I_0(n)+a_8I_1(n)+a_7I_2(n)+a_9I_3(n)+\frac{1}{n}\right]\\&+c_4\left[\left(\frac{1}{n}-a_7\right)K_0(n)+a_8K_1(n)-a_7K_2(n)+a_9K_3(n)\right]-\frac{P}{n^2}a_{10},\end{aligned} \tag{36}$$

$$c_5=\frac{[1-I_0(x_1)]}{n}(c_1-c_3)-\frac{c_4K_0(x_1)}{n}-\frac{P\log x_0}{n^2}+c_6, \tag{37}$$

where

$$\begin{aligned}&a_1=\frac{1}{24}nt^2C_{MQ}-\frac{1}{24}ntC_{MM},\quad a_2=\left(\frac{1}{16}n^2-\frac{1}{12}\right)t^2C_{MQ}-\frac{1}{12}tv_fC_{MM}-1,\\ &a_3=\frac{1}{48}n^2t^2C_{MQ},\quad a_4=\frac{1}{12}(1-v_f)tC_{MM}-1,\\ &a_5=\left(\frac{1}{16}n^2+\frac{1}{12}\right)t^2C_{MQ}+\frac{1}{12}tv_fC_{MM}+1,\\ &a_6=1-\frac{1}{12}(1-v_f)tC_{MM},\quad a_7=\frac{1}{24}nt^3C_{QQ}-\frac{1}{24}nt^2C_{MQ},\\ &a_8=\left(\frac{1}{16}n^2-\frac{1}{12}\right)t^3C_{QQ}-\frac{1}{12}v_ft^2C_{MQ},\quad a_9=\frac{1}{48}n^2t^3C_{QQ},\\ &a_{10}=\frac{1}{12}(1-v_f)t^2C_{MQ},\quad a_{11}=\left(\frac{1}{16}n^2+\frac{1}{12}\right)t^3C_{QQ}+\frac{1}{12}v_ft^2C_{MQ}.\end{aligned} \tag{38}$$

5.3. Special cases for b = 0

When $b=0$, the applied ring load becomes a concentrated load. The governing equation, which is similar to Eq. (27), can be written as

$$x^2\frac{d^2\varphi}{dx^2}+x\frac{d\varphi}{dx}-(1+n^2x^2)\varphi=xP. \tag{39}$$

Thus, the rotation for a deformable substrate is simplified to

$$\varphi=c_7I_1(nx)+c_8K_1(nx)-\frac{P}{n^2x}, \tag{40}$$

where

$$c_8=\frac{P}{n}, \tag{41a}$$

$$c_7=\frac{\frac{P}{n}\left[a_1K_0(n)-a_2K_1(n)+a_1K_2(n)-a_3K_3(n)+\frac{a_4}{n}\right]}{a_1I_0(n)+a_2I_1(n)+a_1I_2(n)+a_3I_3(n)}. \tag{41b}$$

The deflection is deduced to be

$$W=c_7\frac{-1+I_0(nx)}{n}-c_8\frac{K_0(nx)}{n}-\frac{P\log x}{n^2}+c_9,\quad (N_0>0), \tag{42}$$

where the constant c_9 is given by

$$c_9 = c_7\left[\left(-\frac{1}{n}+a_7\right)I_0(n)+a_8I_1(n)+a_7I_2(n)+a_9I_3(n)+\frac{1}{n}\right] + c_8\left[\left(\frac{1}{n}-a_7\right)K_0(n)+a_8K_1(n)-a_7K_2(n)+a_9K_3(n)\right]-\frac{P}{n^2}a_{10}. \quad (43)$$

Furthermore, the above solution is reduced to that given in Wan et al. (2003) when all the compliance coefficients vanish. In this case, the boundary conditions correspond to the clamped boundary conditions, i.e., the substrate is rigid. The deflection at $x = 0$ is given by

$$W|_{x=0} = \frac{P}{n^2}\left\{\frac{1-nK_1(n)}{nI_1(n)}[1-I_0(n)]+K_0(n)+0.577216+\log\frac{n}{2}\right\}, \quad (N_0 > 0), \quad (44)$$

which is consistent with that obtained in Wan et al. (2003).

Finite element analysis (FEA) was performed so as to compare results with the derived analytical solutions. The element mesh is shown in Fig. 3. Axisymmetric, PLANE82 elements in ANSYS were adopted to model the film/substrate systems. The substrate size is 100 times larger than that of the blister. The film thickness is 0.5 mm for this analysis. A Young's modulus of 110 GPa and Poisson ratio of 0.33 were used to simulate the silicon substrate. Thus, Young's modulus of the film is determined by a given value of parameter α. Fig. 4 plots the dimensionless deflection at the center point under the normalized concentrated load for $a/h = 15$. It shows that the analytical solutions compare favorably with FEM.

In the regime of small deflections, the deflection–load relation is linear as shown in Fig. 4. The dimensionless compliance coefficient $k = W/P$ is 0.207, 0.140, 0.132 and 0.125, respectively, for $\alpha = 0.99$, 0.50, −0.50 and −1.0. The results demonstrate that the elastic substrate deformation has a significant effect on the solution if the substrate is softer than the film. It should be pointed out that the dimensionless load P is normalized in Eq. (22a), which is not only related to the load P_0, but also Young's modulus and film dimension.

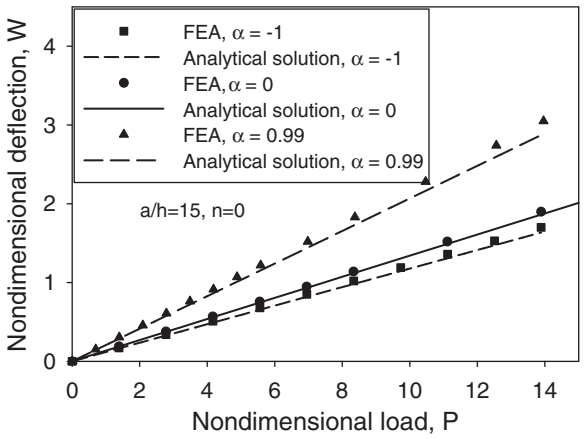

Fig. 4. Comparison between the analytical solution and finite element analysis for small deflection.

6. Numerical solution for the case of large deflection

If the applied load is sufficiently large, the governing equations are nonlinear and, thus, result in a nonlinear deflection–load relation. For large deflections, the shooting method is used to numerically solve the associated nonlinear problem. The initial conditions at the film center are assumed to be

$$\varphi = 0, \quad \frac{d\Delta N}{dx} = 0, \quad \Delta N = \chi, \quad W = \eta, \quad \frac{d\varphi}{dx} = \zeta, \quad \text{at } x = 0. \quad (45)$$

The solution to Eq. (23) subject to the boundary conditions in Eq. (45) can be expressed by

$$\Delta N = \Delta N(x,\chi,\eta,\zeta), \quad W = W(x,\chi,\eta,\zeta), \quad \varphi = \varphi(x,\chi,\eta,\zeta), \quad (46)$$

which must satisfy the boundary conditions given in Eq. (24), i.e.,

$$\begin{aligned} f_1(\chi,\eta,\zeta) &= \left[\Delta N' + C_1\Delta N - C_2P + C_3(\varphi' + v_f\varphi)\right]_{x=1} = 0,\\ f_2(\chi,\eta,\zeta) &= \left[W + C_4\Delta N - C_5P + C_6(\varphi' + v_f\varphi)\right]_{x=1} = 0,\\ f_3(\chi,\eta,\zeta) &= \left[\varphi + C_7\Delta N - C_8P + C_9(\varphi' + v_f\varphi)\right]_{x=1} = 0. \end{aligned} \quad (47)$$

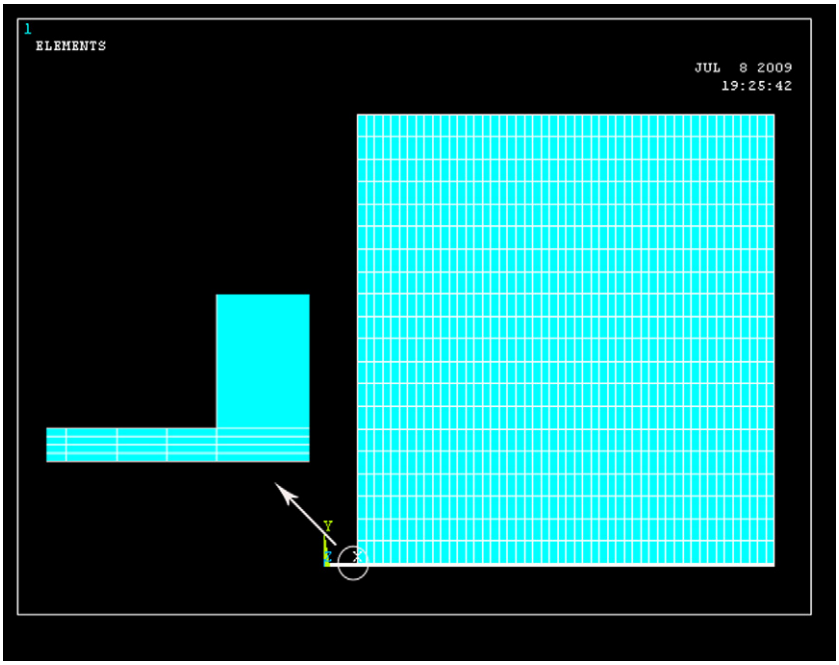

Fig. 3. A typical element mesh.

The values of χ, η and ζ are determined using the following Newton–Raphson iterative approach:

$$\begin{bmatrix} \chi^{(k+1)} \\ \eta^{(k+1)} \\ \zeta^{(k+1)} \end{bmatrix} = \begin{bmatrix} \chi^{(k)} \\ \eta^{(k)} \\ \zeta^{(k)} \end{bmatrix} + \begin{bmatrix} \delta\chi^{(k+1)} \\ \delta\eta^{(k+1)} \\ \delta\zeta^{(k+1)} \end{bmatrix}, \tag{48a}$$

$$\begin{bmatrix} \frac{\partial f_1}{\partial \chi} & \frac{\partial f_1}{\partial \eta} & \frac{\partial f_1}{\partial \zeta} \\ \frac{\partial f_2}{\partial \chi} & \frac{\partial f_2}{\partial \eta} & \frac{\partial f_2}{\partial \zeta} \\ \frac{\partial f_3}{\partial \chi} & \frac{\partial f_3}{\partial \eta} & \frac{\partial f_3}{\partial \zeta} \end{bmatrix} \begin{bmatrix} \delta\chi^{(k+1)} \\ \delta\eta^{(k+1)} \\ \delta\zeta^{(k+1)} \end{bmatrix} = - \begin{bmatrix} f_1^{(k+1)} \\ f_2^{(k+1)} \\ f_3^{(k+1)} \end{bmatrix}, \tag{48b}$$

whereby the solution is found when a preset accuracy criterion is satisfied, i.e.,

$$\text{del} = \left|f_1^{(n)}\right| + \left|f_2^{(n)}\right| + \left|f_3^{(n)}\right| < \Delta, \tag{49}$$

where Δ is a small positive quantity. In the present paper, we take $\Delta = 10^{-6}$. The functions $f_1(\chi,\eta,\zeta)$, $f_2(\chi,\eta,\zeta)$ and $f_3(\chi,\eta,\zeta)$ cannot be expressed in explicit forms, so all calculations are numerical.

Fig. 5 shows the deflections at the contact ring $x = x_0$ obtained by numerical methods and the finite element results for $a/h = 20$, $\alpha = 0$, $x_0 = 0.2$ and $n_0 = 0$. The analytical linear solution for small deflections is also plotted. It can be seen that the numerical results compare favorably with FEM. For $P \leqslant 7$, the analytical solution for small deflection has sufficient accuracy with the relative error being less than 5%. However, when $P > 7$, the large deflection solution must be used in considering nonlinearity. The relative error between the analytical solution and FEM is about 5.3%. In FEM, axisymmetric PLANE82 elements in ANSYS were used, while the nonlinear analytical solution is based on the plate theory. This may be a source of the discrepancy between the two results.

Fig. 6 plots the normalized deflection W versus the normalized load P for different residual stress for $a/h = 10$ and $\alpha = 0.5$. The results demonstrate that the residual stress in the film greatly affects the deflection–load relation where larger residual stresses correspond to smaller deflections.

The effect of substrate properties on the deflection is shown in Fig. 7 for differing Dundurs parameter α. Here, the softer the substrate is, the larger the deflection is. This shows that the substrate deformation cannot be ignored especially for soft substrates. The influence of the shaft radius on the deflection–load relation is demonstrated in Fig. 8. Larger indenter radii lead to smaller deflection.

The effect of parameter a/h is depicted in Fig. 9. We see similarly that, for a given normalized load P, a larger ratio a/h yields a smaller deflection W. When the radius-thickness ratio is large enough,

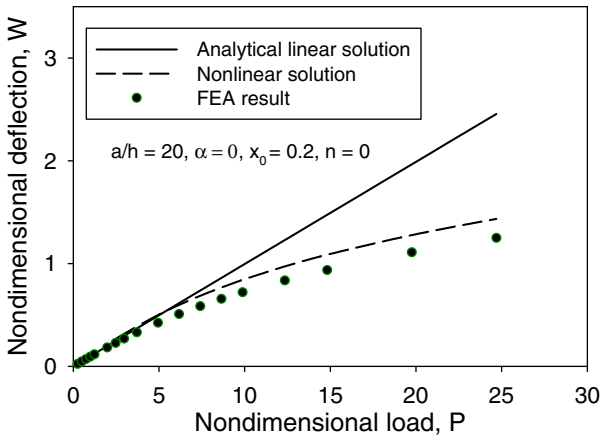

Fig. 5. Deflection at the contact ring $x = x_0$ versus load by numerical method and the finite element analysis.

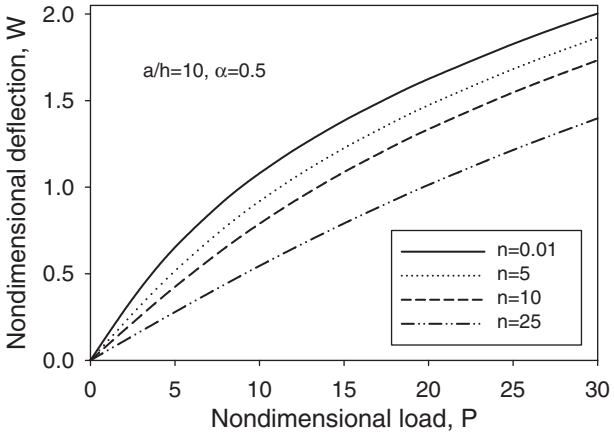

Fig. 6. Influence of residual stress on the deflection–load curve at center point for $a/h = 10$, $\alpha = 0.5$ and $b = 0$.

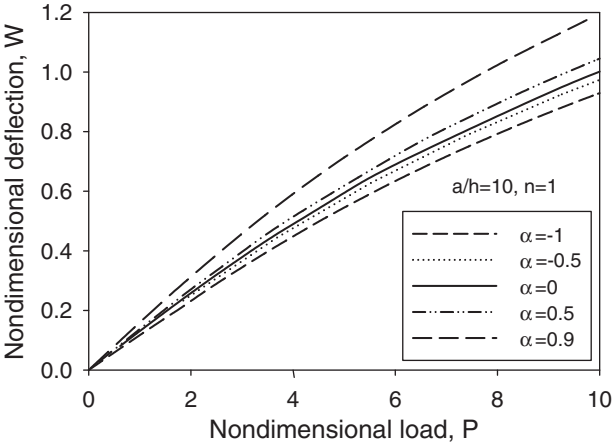

Fig. 7. Influence of elastic mismatch between film and substrate on deflection–load curve at center point for $a/h = 10$, $n = 1$ and $b = 0$.

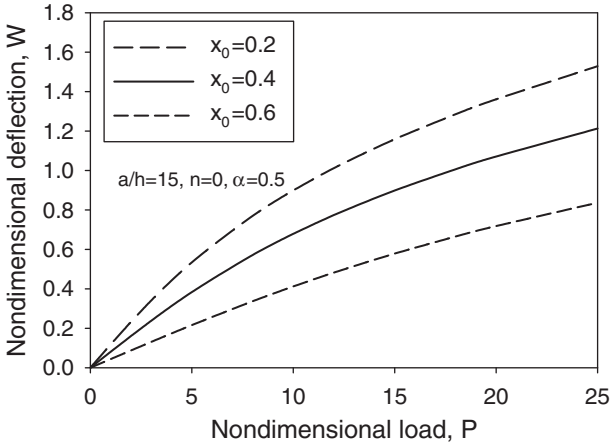

Fig. 8. Deflection–load curves at x_0 for $a/h = 15$, $\alpha = 0.5$ and $n = 0$.

i.e., $a/h \geqslant 500$, the influence can be ignored. The normalized load P is given in Eq. (22a), and is related to the load P_0, Young's modulus and film dimension. Fig. 10 displays the variation in the discrepancy of the deflections for $\alpha = -1$, 0.5 and 0.99 with a/h while the normalized load is set at $P = 6$ and 18. The elastic deformation greatly affects the deflection for small a/h. However, the

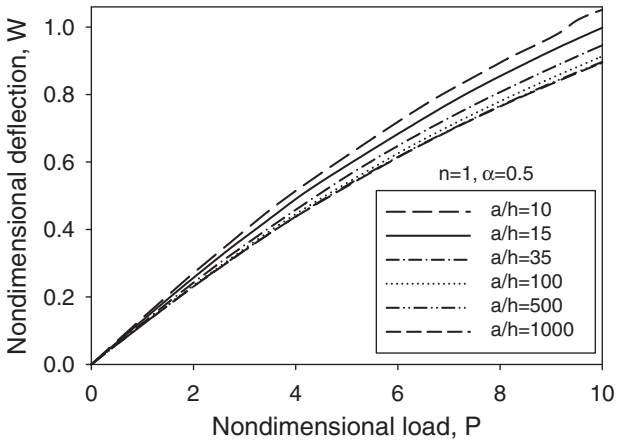

Fig. 9. Normalized deflection–load curves at center point for different a/h for $n = 1$, $\alpha = 0.5$ and $b = 0$.

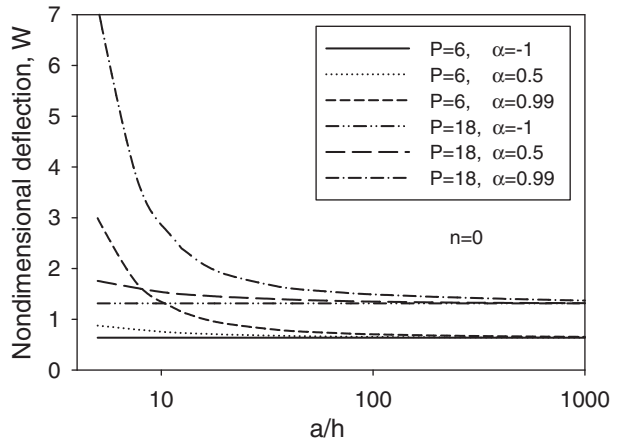

Fig. 10. Variation of the discrepancy of deflections for $\alpha = -1$, 0.5 and 0.99 versus a/h with the given normalized load $P = 6$ and 18.

discrepancy decreases with increasing a/h and all curves converge to that for a rigid substrate at the given load.

7. Concluding remarks

Solutions describing the mechanics of the shaft-loaded blister test method have been obtained, in which the effects and influences of elastic substrate deformation, residual stress, shaft radius, film dimension and elastic properties of thin film have been taken into consideration. The solutions compare favorably with finite element analysis. For small deflections, the solution has been derived in analytical form, and the obtained load–deflection relation is very useful in extracting values for Young's modulus and residual stress of thin films from experimental data. The solution for large deflections has been obtained by a numerical method. The solution is essential in obtaining values for the interfacial fracture toughness of film/substrate systems such as in the blister method given by Xiao et al. (2009). This is because the deflection of the loaded film is usually in the large deflection regime when debonding between the film and the substrate occurs as schematically shown in Fig. 1c. In this type of testing method, we can use the solution of the present paper to calculate the bending moment M and the radial force N at the delamination edge by taking the dimension $a_N = a + \Delta a$ of the newly formed blister. Thereby, the interfacial fracture toughness can be determined by using formulae given by Zhao et al. (2007b).

Acknowledgements

This work was supported by the National Natural Science Foundation of China (No. 10872184) and the Innovation Scientists and Technicians Troop Construction Projects of Henan Province (No. 084200510004) and Program for Innovative Research Team (in Science and Technology) in University of Henan Province (No. 2010IRTSTHN013). The authors would like to acknowledge Mr. Jian Zhou for providing the values of compliances C_{ij}.

Appendix: The empirical expression for the dimensionless compliance coefficients

Using the approach in Zhao et al. (2007b), the dimensionless compliance coefficients in Eq. (12) can be obtained and expressed as:

$$C_{NN} = \frac{1}{1-\alpha}\left(\frac{c_{11}}{c_{12}+h/a}+\frac{c_{13}}{c_{14}+h/a}\right), \tag{A1}$$

$$C_{NM} = C_{MN} = \frac{c_{21}(a/h)}{c_{22}+a/h}+\frac{c_{23}(a/h)}{c_{24}+a/h}, \tag{A2}$$

$$C_{NQ} = C_{QN} = -\frac{c_{31}(a/h)}{c_{32}+a/h}, \tag{A3}$$

$$C_{QQ} = \frac{c_{41}+a/h}{c_{42}+c_{43}(a/h)}, \tag{A4}$$

$$C_{QM} = C_{MQ} = \frac{c_{51}+a/h}{c_{52}+c_{53}(a/h)}. \tag{A5}$$

where the coefficient c_{lk} depends on parameter α as given in Tables 1–5. The compliance C_{MM} is almost independent of a/h and its values are listed in Table 6.

Table 1
Coefficients c_{1k} in Eq. (A1).

α	c_{11}	c_{12}	c_{13}	c_{14}
−0.5	2.3717	1.0412	0.0299	0.0286
0.0	1.4307	0.5576	0.0555	0.0271
0.5	0.6584	0.2629	0.0627	0.0214
0.9	0.1066	0.0633	0.0364	0.0108
0.95	0.0456	0.0359	0.0258	0.0076
0.99	0.0044	0.0017	0.0099	0.0066

Table 2
Coefficients c_{2k} in Eq. (A2).

α	c_{21}	c_{22}	c_{23}	c_{24}
−0.5	0.8151	0.5067	0.7612	0.5067
0.0	0.8234	0.8221	0.8643	0.8221
0.5	0.9319	1.6341	0.9718	1.6340
0.9	1.1986	6.1133	1.2313	6.1133
0.95	1.2158	9.9553	1.4065	9.9553
0.99	1.1579	25.1142	1.6475	25.1144

Table 3
Coefficients c_{3k} in Eq. (A3).

α	c_{31}	c_{32}
−0.5	0.5227	0.6197
0.0	1.1482	1.2582
0.5	2.5824	2.9987
0.9	11.1879	15.3955
0.95	20.5048	29.8270
0.99	98.5638	161.3140

Table 4
Coefficients c_{4k} in Eq. (A4).

α	c_{41}	c_{42}	c_{43}
−0.5	3.2296	2.6377	0.4341
0.0	2.4020	0.8990	0.1618
0.5	1.8610	0.3154	0.0582
0.9	1.3680	0.0583	0.0101
0.95	1.0770	0.0291	0.0051
0.99	0.2358	0.0058	0.0011

Table 5
Coefficients c_{5k} in Eq. (A5).

α	c_{51}	c_{52}	c_{53}
−0.5	−1.3510	1.3690	−1.1520
0.0	−1.2606	0.5318	−0.5062
0.5	−1.0730	0.1736	−0.2233
0.9	−1.0355	0.0357	−0.0596
0.95	−1.1698	0.0243	−0.0362
0.99	−1.3219	0.0047	−0.0118

Table 6
Compliances C_{MM}.

α	−0.5	0.0	0.5	0.9	0.95	0.99
C_{MM}	5.15	7.0	9.9	18.7	24.0	41.7

References

Antunes, J.M., Fernandes, J.V., Sakharova, N.A., Oliveira, M.C., Menezes, L.F., 2007. On the determination of the Young's modulus of thin films using indentation test. International Journal of Solids and Structures 44, 8313–8334.

Cotterell, B., Chen, Z., 2000. Buckling and cracking of thin films on compliant substrates under compression. International Journal of Fracture 104, 169–179.

Dannenberg, H., 1961. Measurement of adhesion by a blister method. International Journal of Applied Polymer Science 5, 125–134.

Föppl, A., 1907. Vorlesungen über Technische Mechanik. Bd. 3. B.G. Teubner, Leipzig.

Hencky, H., 1915. On the stress state in circular plates with vanishing bending stiffness. Zeitschrift fur Mathematik und Physik 63, 311–317.

Jin, C., 2008. Analysis of energy release rate and bending-to-stretching behavior in the shaft-loaded blister test. International Journal of Solids and Structures 45, 6485–6500.

Jin, C., Wang, X.D., 2008. A theoretical study of a thin-film delamination using shaft-loaded blister test: constitutive relation without delamination. Journal of the Mechanics and Physics of Solids 56, 2815–2831.

Kozlova, O., Braccini, M., Eustathopoulos, N., Devismes, M.F., Dupeux, M., 2008. Shaft loaded blister test for metal/ceramic brazing fracture. Materials Letters 62, 3626–3628.

Lai, Y.H., Dillard, D., 1994. A study of the fracture efficiency parameter of blister tests for films and coatings. Journal of Adhesion Science and Technology 8, 663–678.

Li, J.K., Chou, T.W., 1997. Elastic field of a thin-film/substrate system under an axisymmetric loading. International Journal of Solids and Structures 34, 4463–4478.

Marshall, D.B., Evens, G., 1984. Measurement of adherence of residually stressed thin films by indentation. Mechanics of interface delamination. Journal of Applied Physics 58, 2632–2638.

Pharr, C.M., Oliver, W.C., 1992. Measurement of thin film mechanical properties using nanoindentation. MRS Bulletin 17 (7), 34–45.

Randall, N.X., Favaro, G., Frankel, C.H., 2001. The effect of intrinsic parameters on the critical load as measured with the scratch test method. Surface and Coatings Technology 137, 146–151.

Volinsky, A.A., Moody, N.R., Gerberich, W.W., 2002. Interfacial toughness measurements for thin films on substrates. Acta Materialia 50, 441–466.

Wan, K.T., 1999. Fracture mechanics of a shaft-loaded blister test—transition from a bending plate to a stretching membrane. Journal of Adhesion 70, 209–219.

Wan, K.T., Liao, K., 1999. Measuring mechanical properties of thin flexible films by a shaft-loaded blister test. Thin Solid Films 352, 167–172.

Wan, K.T., Guo, S., Dillard, D., 2003. A theoretical and numerical study of a thin clamped circular film under an external load in the presence of residual stress. Thin Solid Films 425, 150–162.

Weihs, T.P., Hong, S., Bravman, J.C., Nix, W.D., 1988. Mechanical deflection of cantilever microbeams: a new technique for testing the mechanical properties of thin films. Journal of Materials Research 3, 931–942.

Williams, M.L., 1969. The continuum interpretation for fracture and adhesion. Journal of Applied Polymer Science 13, 29–40.

Xiao, L.H., Su, X.P., Wang, J.H., Zhou, Y.C., 2009. A novel blister test to evaluate the interface strength between nickel coating and low carbon steel substrate. Materials Science and Engineering A 501, 235–241.

Xu, X.J., Christopher, S., Liao, K., 2003. A shaft-loaded blister test for elastic response and delamination behavior of thin film–substrate system. Thin Solid Films 42, 115–119.

Yu, H.H., Hutchinson, J.W., 2002. Influence of substrate compliance on buckling delamination of thin films. International Journal of Fracture 113, 39–55.

Zhang, T.Y., Su, Y.J., Qian, C.F., Zhao, M.H., Chen, L.Q., 2000a. Microbridge testing of silicon nitride thin films deposited on silicon wafers. Acta Materialia 48, 2843–2857.

Zhang, T.Y., Zhao, M.H., Qian, C.F., 2000b. Effect of substrate deformation on the micro-cantilever beam-bending test. Journal of Materials Research 15, 1868–1871.

Zhao, M.H., Yang, F., Zhang, T.Y., 2007a. Delamination buckling in the microwedge indentation of a thin film on an elastically deformable substrate. Mechanics of Materials 39, 881–892.

Zhao, M.H., Zhou, J., Yang, F., Liu, T., Zhang, T.Y., 2007b. Effects of substrate compliance on the circular buckle delamination of thin films. Engineering Fracture Mechanics 74 (15), 2334–2351.